

Towards Automated Initial Probe Placement in Transthoracic Teleultrasound Using Human Mesh and Skeleton Recovery

Yu Chung Lee, David G. Black, Ryan S. Yeung, and Septimiu E. Salcudean

The University of British Columbia, Vancouver, Canada
lycpaul@ece.ubc.ca

Abstract. Cardiac and lung ultrasound are technically demanding because operators must identify patient-specific intercostal acoustic windows and then navigate between standard views by adjusting probe position, rotation, and force across different imaging planes. These challenges are amplified in teleultrasound when a novice or robot faces the difficult task of first placing the probe on the patient without in-person expert assistance. We present a framework for automating Patient registration and anatomy-informed Initial Probe placement Guidance (PIPG) using only RGB images from a calibrated camera. The novice first captures the patient using the camera on a mixed reality (MR) head-mounted display (HMD). An edge server then infers a patient-specific body-surface and skeleton model, with spatial smoothing across multiple views. Using bony landmarks from the predicted skeleton, we estimate the intercostal region and project the guidance back onto the reconstructed body surface. To validate the framework, we overlaid the reconstructed body mesh and the virtual probe pose guidance across multiple transthoracic echocardiography scan planes *in situ* and measured the quantitative placement error. Pilot experiments with healthy volunteers suggest that the proposed probe placement prediction and MR guidance yield consistent initial placement within anatomical variability acceptable for teleultrasound setup. The codebase for the framework is available at: [RELEASED UPON PUBLICATION].

Keywords: Teleultrasound · Augmented Reality · Patient Registration · Human Mesh Recovery · Probe Placement Guidance · FoCUS · POCUS

1 Introduction

Point-of-care ultrasound (POCUS) offers a practical bedside workflow when comprehensive imaging is not immediately available, and focused cardiac ultrasound (FoCUS) targets a subset of views from transthoracic echocardiography (TTE) to support rapid assessment [18]. Common FoCUS cardiac windows include parasternal long axis (PLAX), parasternal short axis (PSAX), apical four-chamber (A4C), subcostal four-chamber, and subcostal inferior vena cava (IVC) views [19], while Lung POCUS involves left and right’s anterior, posterior, and costophrenic views [20]. Operators may reposition the patient between supine and left lateral decubitus to improve acoustic access, and frequently relocate the probe across intercostal spaces while adjusting angulation and rotation.

Teleoperated robotic or teleguided ultrasound systems have been proposed to improve access in remote areas and reduce the need for on-site expertise [7,12]. They allow an expert to supervise a novice through model-mediated behaviors or teleoperate a robotic ultrasound system by a remote expert or autonomously, thereby improving supervision and standardization [7,14,2,22]. However, these systems often assume the bedside healthcare worker can already find a reasonable initial window, whereas in practice, the initial placement is a key bottleneck that significantly delays the experts ability to take over effectively [17]. It is also difficult to initially locate the probe in teleoperated ultrasound on the patient via teleconference, given the limited patient view and the lack of 3D. Recent work has begun to automate parts of the probe initialization problem. The search-based approach [9] uses a predefined search pattern but is inherently view-specific. Point cloud-based approaches [17,15] can infer the chest and patient surface, but are limited to the supine pose and difficult to generalize to other postures due to their inability to handle rotational invariance and the torso’s shape ambiguity. Thus, automating initial POCUS probe placement remains an unsolved problem.

To address this unmet need and streamline the setup process, we propose an augmented reality-based (AR) approach that (i) reconstructs and registers a patient-specific body model from RGB imagery captured by an HMD, (ii) estimates anatomy-referenced landmarks and generates initial probe pose guidance for multiple transthoracic scan planes, specifically for POCUS cardiac and lung ultrasound, and (iii) visualizes guidance *in situ* to support novice setup for most form of teleultrasound system. To our knowledge, this is the first demonstration of AR guidance that leverages a human skeleton model derived from mesh recovery to estimate probe placement across diverse scan planes. In summary, our approach comprises and integrates the following:

- (i) **Human Mesh Recovery**, which, with parametric body models, enables estimation of patient pose and shape from RGB images. We build on recent advances in SAM-based mesh recovery [21,5] and parametric representations such as SMPL/SMPL-X [11,16]. We further infer a biomechanical skeletal structure and localize bony landmarks using the SKEL model, which re-rigs SMPL with an anatomically accurate skeleton [3].
- (ii) **Anatomy-Aware Guidance**, or body-surface constrained guidance, which is relevant when translating predicted poses into actionable contact points on the torso [15,8]. Our work uses reconstructed surface and skeletal landmarks to generate probe placement cues that lie on the patient’s surface and remain consistent across posture changes.
- (ii) **Augmented Reality (AR)** and mixed-reality (MR) remote guidance methodology that can tightly couple an expert and a novice via *in situ* visual cues, enabling hand-over-hand guidance to improve visualization and interaction in teleultrasound [1,2,22].

2 Methods

2.1 Problem Formulation

Given a patient lying on an exam bed in one of several clinically relevant postures (e.g., supine or left lateral decubitus), our objective is to generate an initial POCUS probe placement pose for a set of target transthoracic scan planes. A patient-side novice captures multiple RGB images with a calibrated camera, and the system returns: (a) a registered patient body surface mesh and skeleton model in world coordinates, and (b) a

probe pose for each target scan plane, projected on the recovered patient surface. These outputs are visualized as *in situ* holographic overlays to support initial setup before (or while) the remote expert or the robotic system provides fine guidance.

2.2 System Overview

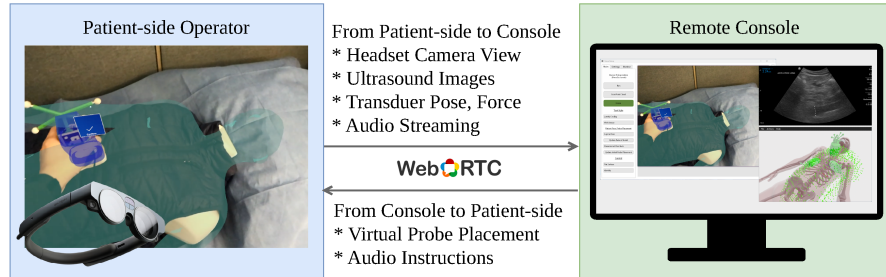


Fig. 1: Teleultrasound’s patient-side and remote console with bidirectional streaming and AR guidance overlays via WebRTC protocol. The remote console end could monitor the examination from the headset’s point-of-view camera and ultrasound video.

Figure 1 illustrates the system architecture. On the patient side, an AR headset (Magic Leap 2) provides first-person view (FPV) camera streams and ultrasound images to the remote console. The headset produces holographic overlays of the virtual probe. We attached ArUco markers on the ultrasound probe for pose measurements and tracking [6]. The remote console runs on a standard office desktop and transfers registration metadata to the edge server. The guidance prediction module, including model inference and optimization, runs on an edge server equipped with an NVIDIA RTX 3090 Ti. Our contribution augments the teleultrasound loop with an automated registration and initial probe placement guidance module that runs after the patient-side operator captures the patient’s imagery.

2.3 Automatic Patient Registration

We estimate a patient-specific body model from RGB images obtained from multiple views and align it to the AR headset coordinate frame.

Coordinate frames. Let $\{W\}$ denote the HMD world frame, with the HMD FPV camera frame $\{C\}$, the reconstructed body/skeleton canonical frame $\{B\}$, and $\{P_i\}$ denote the probe pose of the i th view. The HMD provides the camera pose homogeneous transformation ${}^W\mathbf{T}_C$. A human mesh recovery model predicts a body representation and yields translation and orientation ${}^C\mathbf{T}_B$ with respect to the local camera frame. We obtain the overall patient transformation with ${}^W\mathbf{T}_B = {}^W\mathbf{T}_C {}^C\mathbf{T}_B$ and probe transformation ${}^W\mathbf{T}_P$ from guidance prediction.

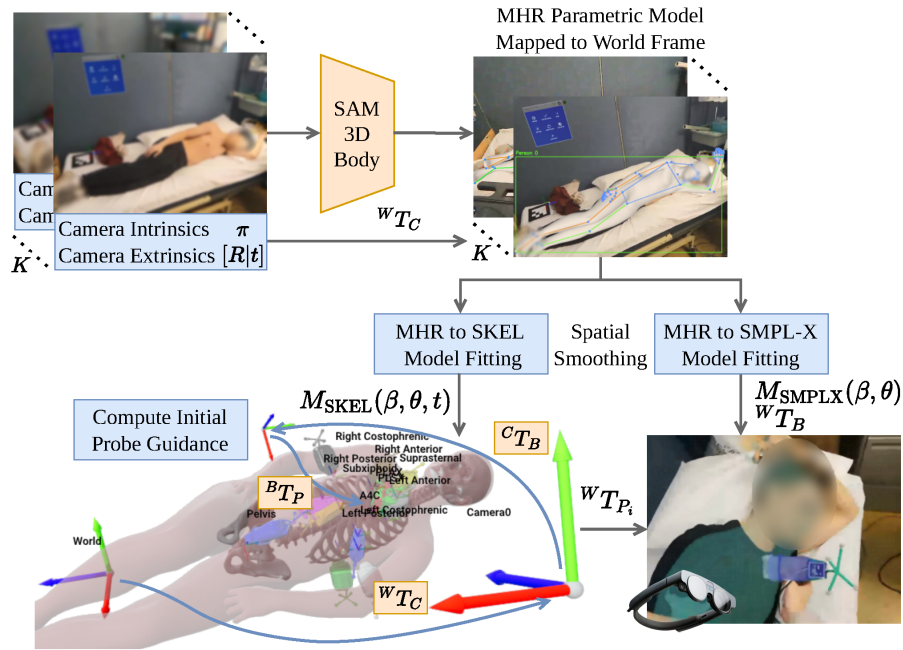


Fig. 2: Overall framework of the proposed patient registration and initial probe placement guidance (PIPG). Given a batch of K images, the system leverages the patient’s spatial consistency to predict the patient’s anatomy and align it with the system’s coordinates for guidance generation.

Body models and parametric conversion. We first used SAM 3D Body [21] to recover 3D human meshes using Momentum Human Rig (MHR) parameters [4]. Camera intrinsics are obtained from the HMD and provided to the model, rather than using the default field-of-view estimator. We convert the MHR model to the SMPL and SMPL-X parametric models, respectively. The SMPL-X model, defined as $M_{\text{SMPLX}}(\beta, \theta, \mathbf{t})$ with shape parameters $\beta \in \mathbb{R}^{10}$, pose parameters $\theta \in \mathbb{R}^{22 \times 3}$, and camera translation $\mathbf{t} \in \mathbb{R}^3$, is used to render the body mesh in the HMD using the SMPLX-Unity library provided by [16]. The SMPL model is used as an intermediate representation for converting to the SKEL skeleton body via optimization, defined as $M_{\text{SKEL}}(\beta, \theta, \mathbf{t})$ with shape parameters $\beta \in \mathbb{R}^{10}$, pose parameters $\theta \in \mathbb{R}^{46}$, and camera translation $\mathbf{t} \in \mathbb{R}^3$. To facilitate the optimization loop, we partially mask vertices and joints, retaining only the torso region when computing the fitting loss. This conversion provides a consistent set of joint locations and bony landmarks for generating downstream probe placements.

Spatial Smoothing via Multi-frame Batch Fitting Single-frame MHR predictions can exhibit pose/shape jitter, leading to unstable predictions. To leverage spatial and temporal consistency, we infer a short batch of $K=8$ frames and fit a single SMPL/SMPL-X instance to the batch after transforming the MHR outputs into the world frame. For each frame i , the HMD provides ${}^W\mathbf{T}_{C_i}$ and MHR yields a body es-

time in the camera frame. We transform the predicted mesh (or joints) into world coordinates and aggregate observations: $\{\mathbf{X}_i^W\}_{i=1}^K \leftarrow \{{}^W\mathbf{T}_{C_i}\mathbf{X}_i^C\}_{i=1}^K$.

To suppress outliers arising from partial views or transient tracking errors, we perform RANSAC-based robust fitting over the batch to select the SMPL and SMPL-X parameters that maximize the support for inliers. The resulting consensus parameters are used as the final spatially consistent body mesh for visualization and for skeleton model inference.

2.4 Probe Placement Guidance Generation

For each target scan plane, we predefine an anatomy-referenced rule that maps skeleton/bony landmarks to an initial probe pose. The transformation from patient body frame to each probe view ${}^B\mathbf{T}_{P_i}$ can be deduced by the following cues: (i) a small set of bony landmarks (e.g., sternum and adjacent rib/intercostal references), (ii) an offset model along the thoracic surface normal, and (iii) a desired probe orientation relative to anatomical axes (e.g., along the pelvis or thoracic axis).

Anatomy-Aware Probe Pose. Let \mathbf{p}_ℓ be a predicted landmark in the body frame and $\hat{\mathbf{n}}(\mathbf{p})$ the outward normal based on the thoracic axis. To ensure that the virtual guidance lies on the patient surface, we compute the final contact point by projecting the landmark along the outward normal to intersect the reconstructed torso surface, and then place the probe at the intersection point with a small inward offset to indicate nominal contact pressure. We further orient each projected probe pose according to POCUS guidelines in [19,20] relative to the body longitudinal axis.

2.5 Runtime Optimization

The current implementation relies on parametric model conversion and optimization-based fitting, which can dominate runtime. To improve efficiency, we parallelize the conversions from MHR to SMPL-X and SKEL. We further speed up the original SKEL fitting by adding caching and reducing per-iteration overhead. Combined with restricting the fitting loss to the torso, the end-to-end runtime of the pipeline in Figure 2 is reduced to approximately 40 s in our system, compared with roughly 2 min reported in related work [15].

3 Experiments

We conducted pilot experiments with healthy volunteers in two postures: supine and left lateral decubitus. The novice user wore an AR headset (Magic Leap 2) and captured eight RGB images of the patient, each with an associated camera pose and parameters. We then generated and visualized initial probe guidance for selected cardiac and lung windows in each posture. The novice user was asked to follow the visual guidance, maneuvering the probe to align with the suggested pose while maintaining contact between the transducer and the patients body surface. We recorded the resulting probe pose as the *guided pose*. To obtain a reference, we positioned the probe at the upper and lower sternum landmarks and recorded these as the *ground-truth anatomical pose*, as these

landmarks are most palpable and exhibit the least ambiguity. We recruited five healthy volunteers as patients (five male, height 181.5 ± 4.5 cm, weight 76 ± 8 kg, age 26 ± 3 years), three of whom also served as novice users. We further analyze the results based on the following three comparison metrics:

a. Guided Pose p_{guided} vs. Prediction p_{pred} (depth and surface prediction error). The novice user was instructed to align a physical probe with the predicted pose and advance it toward the patient until it contacted the skin with slight pressure. We measure the discrepancy between the AR-guided contact point and the predicted probe position, thereby capturing offsets in surface mesh recovery and depth estimation. Based on the accessibility and representativeness of each view, we measured the suprasternal long-axis, subcostal four-chamber, right and left anterior, and costophrenic angle views in the supine posture to cover various thoracic regions. In left lateral decubitus, the apical four-chamber and left costophrenic views were omitted because they were inaccessible in our setup.

b. Prediction p_{pred} vs. Ground Truth p_{gt} (anatomy alignment). The operator and patient identified palpable landmarks (the upper and lower sternum) and placed the probe accordingly. We measure how well the predicted anatomical landmarks align with the ground-truth reference. When locating the upper sternum, the operator orients the probe normal to the torso surface and aligns the image plane to the longitudinal axis. The recorded probe rotation is used as the ground-truth torso rotation to compute the tilt and spin errors.

c. Guided Pose p_{guided} vs. Ground Truth p_{gt} (task-level utility). We compare the novices final probe placement when following AR guidance to the ground-truth target location to assess whether the guidance helps approach the intended anatomy. Here, we use the guided poses for the suprasternal long-axis and subcostal four-chamber views, as they are proximal to the upper and lower sternum, respectively.

For each probe pose comparison, we report the Euclidean distance as the positional error e_{pos} , the tilt error e_{tilt} , and the spin error e_{spin} . Defining the probe normal of probe pose p_{probe} be $\mathbf{n}_{probe} = R_{probe}\hat{\mathbf{z}}$, and the view plane normal denoted as $\mathbf{x}_{probe} = R_{probe}\hat{\mathbf{x}}$, the spin error is computed by projecting the view plane normal to the thoracic reference plane π_{thorax} with normal $\mathbf{n}_{thorax} = R_{thorax}\hat{\mathbf{z}}$, where R_{thorax} obtained by the mesh recovery. We then compute all errors of two probe pose pair as $e_{pos} = \|p_a - p_b\|_2$, $e_{tilt} = \cos^{-1}(\mathbf{n}_a^\top \mathbf{n}_b)$, and $e_{spin} = \cos^{-1}((\text{proj}_{\pi_{thorax}} \mathbf{x}_a)^\top (\text{proj}_{\pi_{thorax}} \mathbf{x}_b))$.

4 Results and Discussion

Figures 4 and Table 1 show consistent trends across postures and subjects. In both the supine and left lateral decubitus positions, the guided-to-prediction error has a mean of 16–18 mm, indicating that the predicted body surface closely encloses the patient’s body and that novices can reliably follow the AR overlay while keeping the probe in contact. While occasional larger outliers are expected, the subject-level means indicate that average performance per scan is consistent. The prediction-to-ground-truth error mean is consistently in the mid-20 mm range, with the overall distribution spanning 18–33 mm. The guided-to-ground-truth error means are close to the prediction-to-ground-truth error with a wider distribution, suggesting that the dominant source of error is

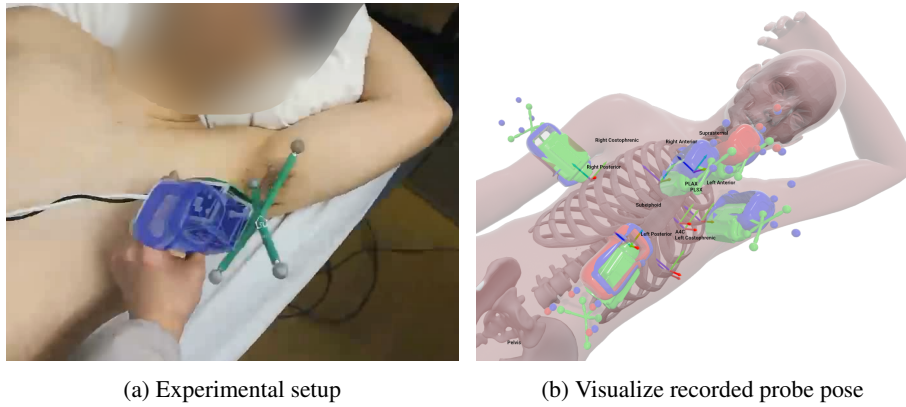


Fig. 3: (a) first-person view from the AR headset during probe tracking and guidance following. (b) Predicted pose is rendered in green, guided pose is in blue, and red indicates the ground-truth pose (upper and lower sternum).

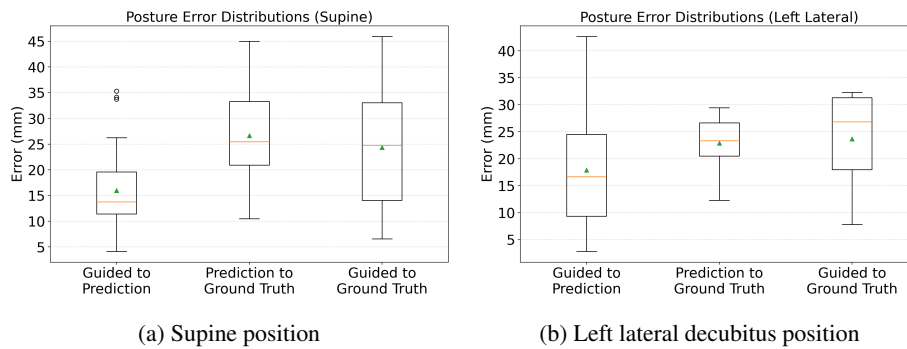


Fig. 4: (a) Error distribution across all views in supine position. (b) and the left lateral decubitus position. Detailed statistics are summarized in Table 1.

anatomical alignment, although user compliance with the guidance may still vary. Both tilt and spin orientation mean errors are within 3–7 degrees across different pose comparison metrics, indicating that the novice can accurately follow the guidance’s angulation and that the predicted torso orientation is aligned with the actual patient’s posture.

Guidance Utility for Initial Placement. Beyond absolute error, we consider whether the proposed guidance reaches an accuracy range that is practically meaningful for novice setup. Prior FoCUS training study reports that untrained physicians exhibit a median probe placement error of 3.2 cm and 3.1 cm after training with a simulator[13]. Our pilot results suggest that the proposed AR guidance can achieve placement errors within this range, supporting the hypothesis that it can provide a clinically viable “warm start” prior to expert fine guidance. Future studies will quantify gains in consistency across novices and trials and evaluate downstream outcomes, such as time-to-first-diagnostic

Table 1: Error distribution reported as Mean \pm Standard Deviation.

Metrics	$P_{\text{guided}}-P_{\text{pred}}$	$P_{\text{pred}}-P_{\text{gt}}$	$P_{\text{guided}}-P_{\text{gt}}$
Supine position (mm) e_{pos}	16.0 ± 8.02	26.7 ± 8.95	24.4 ± 11.5
Left lateral decubitus (mm) e_{pos}	17.9 ± 9.85	22.9 ± 5.04	23.7 ± 8.96
Subject-level mean (mm) e_{pos}	16.9 ± 4.07	24.8 ± 6.29	24.0 ± 7.88
Overall positional errors (mm) e_{pos}	16.8 ± 8.88	25.1 ± 7.85	24.1 ± 10.6
Overall tilt errors (deg) e_{tilt}	5.64 ± 3.95	6.68 ± 4.19	6.79 ± 3.95
Overall spin errors (deg) e_{spin}	2.95 ± 2.40	3.67 ± 2.77	4.87 ± 2.77

view, displacement from the standard view location, and ultrasound image comparison between the predicted window and the standard view.

Our pilot findings suggest that anatomy-informed AR overlays can improve the setup phase of transthoracic teleultrasound by providing a consistent initial probe placement on the patient surface, anchored to predicted thoracic intercostal landmarks. This addresses a practical challenge in teleultrasound workflows, in which novice users struggle to identify initial windows, thereby delaying the experts examination.

Limitations. We chose the SAM 3D Body for its stable, consistent performance in handling depth ambiguity. However, runtime is constrained by model conversion and optimization, where direct feedforward skeleton prediction may reduce optimization overhead [10]. Our current registration is a one-off step and does not account for body motion during scanning, and future work should incorporate motion tracking and compensation. Our pilot evaluation with healthy volunteers does not capture clinical variability (gender diversity, body habitus, pathology, challenging windows), motivating broader studies.

5 Conclusion

We presented an AR-based framework for automated patient registration and anatomy-informed initial probe placement guidance for transthoracic cardiac and lung teleultrasound using RGB-based human mesh recovery and skeleton landmarks. By overlaying a registered body surface and plane-specific probe pose guidance *in situ*, the method provides a practical warm start for novice setup before expert takeover. Although the system is designed to use an AR headset as the interface, paired with a freehand ultrasound probe, the proposed PIPG framework is intrinsically system-agnostic and could be adopted in most teleultrasound systems equipped with a calibrated camera (e.g., teleguided, teleoperated, or robotic ultrasound systems) to streamline setup and provide initial placement. Pilot results motivate further clinical validation and downstream evaluation of teleoperated ultrasound using our initial probe placement prediction framework. Future work can focus on evaluating clinically meaningful endpoints, such as time-to-first-diagnostic view and image quality, under expert supervision, and on extending guidance rules to additional planes and patient positions. We will also explore personalized and semi-autonomous probe guidance by using predicted surface/skeleton features as priors to locate optimal acoustic windows.

Disclosure of Interests. The authors have no competing interests to declare that are relevant to the content of this article.

References

1. Black, D., Salcudean, S.: Robotic versus Human Teleoperation for Remote Ultrasound. Hamlyn Symposium for Medical Robotics (2025)
2. Black, D.G., Salcudean, S.E.: Stability and transparency in mixed-reality bilateral human teleoperation. *IEEE Transactions on Robotics* **41**, 5800–5815 (2025)
3. Dakri, A., Arora, V., Challier, L., Keller, M., Black, M.J., Pujades, S.: On Predicting 3D Bone Locations Inside the Human Body. In: Linguraru, M.G., Dou, Q., Feragen, A., Giannarou, S., Glocker, B., Lekadir, K., Schnabel, J.A. (eds.) *Medical Image Computing and Computer Assisted Intervention MICCAI 2024*, vol. 15003, pp. 336–346. Springer Nature Switzerland, Cham (2024)
4. Ferguson, A., Osman, A.A.A., Bescos, B., Stoll, C., Twigg, C., Lassner, C., Otte, D., Vignola, E., Bogó, F., Santesteban, I., Romero, J., Zarate, J., Lee, J., Park, J., Yang, J., Doublestein, J., Venkateshan, K., Kitani, K., Kavan, L., Farra, M.D., Hu, M., Cioffi, M., Fabris, M., Ranieri, M., Modarres, M., Kadlecěk, P., Abdrashitov, R., Prévost, R., Rajbhandari, R., Mallet, R., Pearsall, R., Kao, S., Kumar, S., Parrish, S., Wang, T.L., Tung, T., Dong, Y., Chen, Y., Xu, Y., Ye, Y., Jiang, Z.: MHR: Momentum Human Rig. *arXiv preprint arXiv:2511.15586* (2025)
5. Gao, M., Miao, Y., Han, J.: SAM-Body4D: Training-Free 4D Human Body Mesh Recovery from Videos. *arXiv preprint arXiv:2512.08406* (2025)
6. Garrido-Jurado, S., Muñoz-Salinas, R., Madrid-Cuevas, F.J., Marín-Jiménez, M.J.: Automatic generation and detection of highly reliable fiducial markers under occlusion. *Pattern Recognition* **47**(6), 2280–2292 (2014)
7. Jiang, Z., Salcudean, S.E., Navab, N.: Robotic ultrasound imaging: State-of-the-art and future perspectives. *Medical image analysis* **89**, 102878 (2023)
8. Keller, M., Werling, K., Shin, S., Delp, S., Pujades, S., Liu, C.K., Black, M.J.: From skin to skeleton: Towards biomechanically accurate 3d digital humans. *ACM Trans. Graph.* **42**(6) (2023)
9. Laurent, E., Soemantoro, R., Jenner, K., Kardos, A., Tang, G., Zhao, Y.: Echo-Robot: Semi-Autonomous Cardiac Ultrasound Image Acquisition Using AI and Robotics. *IEEE Transactions on Medical Robotics and Bionics* **7**(3), 1307–1316 (2025)
10. Li, D., Jin, J., Yu, X., Liu, W., Cun, X., Chen, K., Fan, R., Kong, J., Shen, X.: SKEL-CF: Coarse-to-Fine Biomechanical Skeleton and Surface Mesh Recovery. *arXiv preprint arXiv:2511.20157* (2025)
11. Loper, M., Mahmood, N., Romero, J., Pons-Moll, G., Black, M.J.: Smpl: a skinned multi-person linear model. *ACM Trans. Graph.* **34**(6) (2015)
12. Marwick, T.H., Hidalgo, E.M., Wright, L., Roshan, M., Isaksson, M.: Current Status and Pending Developments of Robotic Tele-Echocardiography. *JACC: Cardiovascular Imaging* **18**(12), 1377–1388 (2025)
13. Morgan, Do, R., Sanville, Md, B., Bathula, S., Demirel, PhD, S., Perkins, Md, S., Johnson, Md, G.E.: Simulator-Based Training in FoCUS with Skill-Based Metrics for Feedback: An Efficacy Study. *POCUS Journal* **4**(2), 33–36 (2019)
14. Munir, K., Al-Battal, A.F., Alsheghri, A., Becher, H., Noga, M., Punithakumar, K.: A Survey of Autonomous Robotic Ultrasound Scanning Systems. *IEEE Access* **13**, 103178–103197 (2025)
15. Nardi, D., Lamon, E., Fontanelli, D., Saveriano, M., Palopoli, L.: An Anatomy-Aware Shared Control Approach for Assisted Teleoperation of Lung Ultrasound Examinations. *IEEE Robotics and Automation Letters* **11**(3), 2570–2577 (2026)

16. Pavlakos, G., Choutas, V., Ghorbani, N., Bolkart, T., Osman, A.A., Tzionas, D., Black, M.J.: Expressive Body Capture: 3D Hands, Face, and Body From a Single Image. In: 2019 IEEE/CVF Conference on Computer Vision and Pattern Recognition (CVPR). pp. 10967–10977. IEEE, Long Beach, CA, USA (2019)
17. Roshan, M.C., Hidalgo, E.M., Isaksson, M., Dunn, M., Pyaraka, J.C.: Finding an Initial Probe Pose in Teleoperated Robotic Echocardiography via 2D LiDAR-Based 3D Reconstruction. arXiv preprint arXiv:2509.24867 (2025)
18. Spencer, K.T., Kimura, B.J., Korcarz, C.E., Pellikka, P.A., Rahko, P.S., Siegel, R.J.: Focused Cardiac Ultrasound: Recommendations from the American Society of Echocardiography. *Journal of the American Society of Echocardiography* **26**(6), 567–581 (2013)
19. University Health Network Perioperative Interactive Education (PIE): Focused cardiac ultrasound (focus) (2020), https://pie.med.utoronto.ca/POCUS/POCUS_content/focus.html
20. University Health Network Perioperative Interactive Education (PIE): Lung ultrasound (2020), https://pie.med.utoronto.ca/POCUS/POCUS_content/lungUS.html
21. Yang, X., Kukreja, D., Pinkus, D., Sagar, A., Fan, T., Park, J., Shin, S., Cao, J., Liu, J., Ugrinovic, N., Feiszli, M., Malik, J., Dollar, P., Kitani, K.: Sam 3d body: Robust full-body human mesh recovery. arXiv preprint arXiv:2602.15989 (2026)
22. Yeung, R.S., Black, D.G., Salcudean, S.E.: Measurement and Potential Field-Based Patient Modeling for Model-Mediated Tele-ultrasound. arXiv preprint arXiv:2509.15325 (2025)